RESEARCH PAPER

IJAMB JOURNALAMB.COM
INTERNATIONAL JOURNAL OF ADVANCES IN MEDICAL BIOTECHNOLOGY

3D printed hydroxyapatite-collagen from tilapia skin scaffolds for bone tissue engineering proposals

K. dos S. J. Sousa[1]*; G. M. da Costa[1]; G. O. Amaral[1]; A. C. Renno[1]

*Corresponding author: E-mail address: kksousa12@gmail.com

Received: October 2024; Accepted: December 2024.

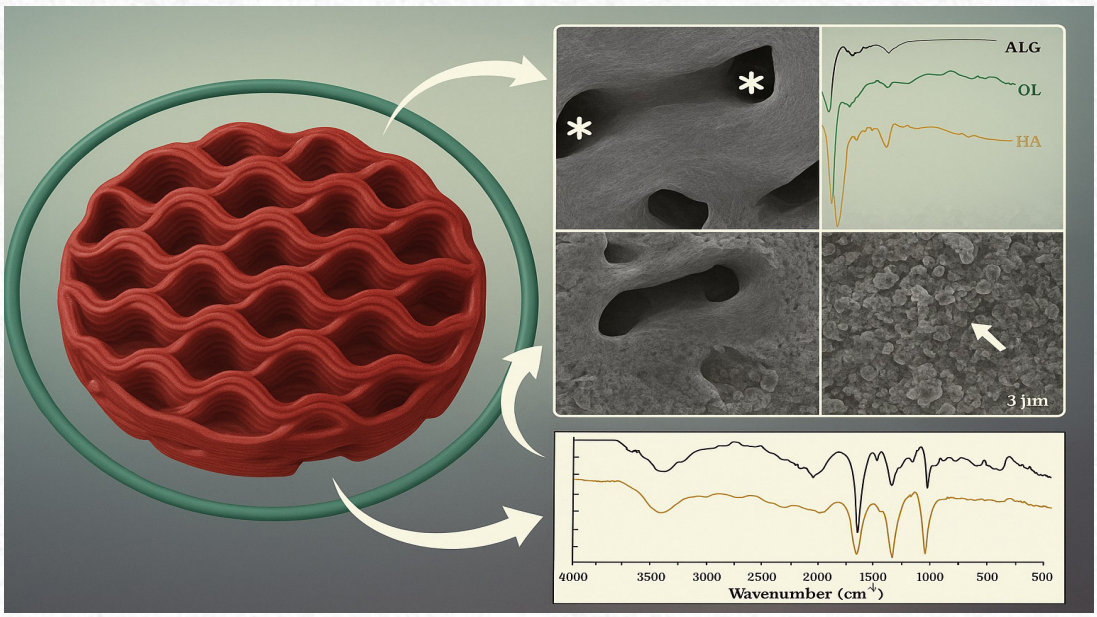

Abstract: Bone possesses an inherent capacity for healing fractures, thereby restoring tissue structure and biomechanical properties. However, conditions such as osteoporosis, tumors, and infections can hinder and prolong the healing process, resulting in non-union fractures. Biomaterials, notably hydroxyapatite (HA) and collagen (Col), play a pivotal role in fracture treatment by fostering bone cell differentiation and new bone formation. HA mimics bone mineral components, while Col represents the organic matrix. Biomimetic scaffolds combining HA/Col, particularly utilizing natural collagen-like that sourced from fish, have garnered attention for their demonstrated osteogenic and angiogenic potential. Additionally, advancements in 3D printing technology enable the fabrication of scaffolds with interconnected pores. This study evaluates the physicochemical properties and cytotoxicity of 3D-printed HA and HA/COL scaffolds. Scanning electron microscopy shows uniformity in HA scaffolds and a fibrous appearance in HA/COL scaffolds. Fourier-transform infrared spectroscopy distinguishes characteristic peaks of HA and COL. Energy-dispersive X-ray spectroscopy reveals varying calcium/phosphate ratios. Over 21 days, mass loss rates, pH, and swelling ratios differ between scaffold types. MTT assay results demonstrate increased cell viability and non-cytotoxicity in HA and HA/COL scaffolds compared to controls, indicating the promise of HA/COL scaffolds for bone regeneration.

Keywords: Hydroxyapatite. Fish collagen. Bone. 3D printed scaffold.

[1]Department of Biosciences, Federal University of São Paulo (UNIFESP), Santos, SP, Brazil.

https://doi.org/10.52466/ijamb.v7i1.151

Introduction

Bone has an intrinsic ability of healing after the occurrence of a fracture, being able of restoring the previous tissue structure and its biomechanical properties [1]. However, under certain circumstances such as the presence of osteoporosis, tumors, diabetes, infections, insufficient blood supply, or extensive fracture size, delayed healing or even nonunion fractures may occur, compromising the process of regeneration[2,3].

In this context, biomaterial-based bone grafts placed at the site of the bone injury have a key role as a therapeutical approach for treating non-consolidated fractures, being able of stimulating bone cell differentiation and newly formed bone deposition, accelerating the process of healing [4]. Bone grafts can be constructed using a variety of materials, such as metals, ceramics, and polymers, known for their exceptional biocompatibility with the organism and osteogenic properties, being able of stimulating bone ingrowth[5–7]it is a very dynamic tissue subjected to continuous remodeling in order to preserve its structure and function. However, in clinical practice, impaired bone healing can be observed in patients and medical intervention is needed to regenerate the tissue via the use of natural bone grafts or synthetic bone grafts. The main elements required for tissue engineering include cells, growth factors and a scaffold material to support them. Three different materials (metals, ceramics, and polymers.

One of the most prominent biomaterial used for this proposal is the hydroxyapatite (HA)[8]. HA has been widely used as a base material to for manufacturing scaffolds due to its structural and chemical similarity to the mineral elements of the bone itself. HA shows good osteoconductive properties, being able of stimulating osteoblasts proliferation, and tissue ingrowth at the site of the fracture[9–13]. However, the degradation index which might not align with the rate of bone regeneration in some cases, and low mechanical properties constitute disadvantages for this material, mainly for its long-term use in bone tissue[14].

In this context, combining different materials can yield improved biological performance for treating bone fractures[15,16]. Therefore, one of the most common material options is the inclusion of collagen (Col) into HA[17–19]an abundant extracellular matrix protein, has been found to have a lot of pharmaceuticals, medicine, food, and cosmetics applications. Increased knowledge of collagen sources, extraction techniques, structure, and properties in the last decades has helped develop more collagen-based products and tissue engineering biomaterials. Collagen products have been playing an important role in benefiting the health of the human body, especially for aging people. In this paper, the effects of collagen treatment in different clinical studies including skin regeneration, bone defects, sarcopenia, wound healing, dental therapy, gastroesophageal reflux, osteoarthritis, and rheumatoid arthritis have been reviewed. The collagen treatments were significant in these clinical studies. In addition, the associations between these diseases were discussed. The comorbidity of these diseases might be closely related to collagen deficiency, and collagen treatment might be a good choice when a patient has more than one of these diseases, including the coronavirus disease 2019 (COVID-19. It is well known that Col can be extracted from different natural sources, with bovine and porcine origins being the most common[20,21]. Although Col is readily available from these sources, the risks of disease transmission, the potential for triggering adverse immune and inflammatory responses, and the high final cost of the product, drive the constant search for alternative natural sources that combine biocompatibility, low cost, availability, and ease of handling[22–24].

One the alternatives is the use of Col from fish species, including golden carp[25], tuna[26,27], sea bass[26], and tilapia[28,29]. The Col obtained from tilapia exhibits amino acid composition, rheological properties, and thermal stability similar to mammalian Col, suggesting its potential as an alternative for biomedical applications[30]. Moreover, the combination of HA with Col has shown promising results in recent studies, resulting in the development of an angiogenic and osteogenic nanocomposite with enhanced mechanical resistance and higher osteogenic properties[12,13,31,32]. According to Kavitha Sri et al. [33], the presence of Col in the composite facilitates cellular attachment and is responsible for osteoblast adsorption and mineral deposition. Additionally, the incorporation of HA also promotes the deposition of minerals.

Also, HA/Col have used for manufacturing scaffolds, which serve as a structural framework for cellular attachment, proliferation, and bone ingrowth [4,34]. One of the most promising techniques used for scaffold manufacturing is the 3D printing[35,36]. It has been emerging as a disruptive technology for producing bone grafts, allowing the control of pore creation and pore interconnectivity[37,38]. Moreover, Xie et al.[39] demonstrated, in animal studies that 3D-manufactured scaffolds composed of HA/COL exhibited an optimal environment for osteoblast adhesion, migration, and growth.

Furthermore, taking into account the scientific, environmental, and economic dimensions, the

fabrication of 3D printed scaffolds employing Col derived from tilapia skin and HA via 3D printing represents a potentially economically viable alternative. Therefore, the hypothesis of this study is that 3D printed HA/Col scaffolds have the potential to be an improved treatment for stimulating bone ingrowth and accelerating fracture consolidation. Thus, the present study aimed to evaluate the physicochemical and morphological properties and the cytotoxicity of 3D printed scaffolds of HA/COL.

Methodology

Materials

Synthetic HA powder (no. 21223-1kg, purity > 90%, $Ca_3(PO_4)_2$) and sodium alginate (ALG) (no. W201502) were purchased from Sigma Aldrich®. Fresh tilapia skin was collected from the Fish Market in Santos (São Paulo, Brazil) and kept on ice until arrival at the laboratory.

Collagen extraction (COL) from tilapia skin

After removing the scales and the meat, tilapia skin was obtained, cut into pieces of 5 cm^2, and washed to remove surface impurities. Afterward, the skin was lyophilized and weighed. Then, COL was extracted using the method described by Li et al. [40], with modifications. Briefly, the skin was kept in a solution of 0.1 M NaOH at a 1:50 (w/v) ratio for 8 hours, under agitation for non-collagenous proteins and pigments removal. The solution was changed every 4 hours. Then, the skin was washed with distilled water until a neutral pH was obtained. Samples were inserted in a solution of 10% (v/v) butyl alcohol at a ratio of 1:50 (w/v) for 24 hours with agitation and renewed every 8 hours for the removal of fat tissue. After this step, samples were carefully washed with distilled water until a neutral pH was obtained, lyophilized, and weighed again. The lyophilized skin samples were then soaked in 0.5 M acetic acid (1:50, w/v) for 48 hours with continuous stirring at 10°C. After stirring, the obtained solution was filtered and the filtrate was stored.

The filtered material was centrifuged at 4800 rpm for 20 minutes at 4 °C. The supernatants were collected and salted with NaCl to a concentration of 0.9 M, homogenized well, and then salted again to 2.4 M with NaCl for collagen precipitation. The supernatants and precipitates were placed in 50 mL falcons and centrifuged at 4800 rpm for 20 minutes. The supernatant was discarded, and the precipitate was collected to be resolubilized in 0.5 M acetic acid. The COL solution was dialyzed with a dialysis membrane (molecular weight cutoff of 30 kDa) against a solution of 0.1 M acetic acid for 48 hours (with a change after 24 hours). Then, the dialysis solution was performed again, with distilled water for 24 hours. The dialyzed material was frozen, lyophilized, and ground using a cryogenic mill to obtain a COL powder (5µm).

Preparation of HA and HA/COL inks

The HA ink was produced by mixing 1.5 g of ALG at 6% (w/v) and 3.49 g of HA at a ratio of ALG/HA (30/70%, w/v) in water (25 mL). The mixture ALG/HA was homogenized in water at a temperature of 55 °C. After the ALG/HA solution reached room temperature, 2% calcium chloride ($CaCl_2$) (5 mL) was added to obtain the primary crosslinking. Then, the ink was kept refrigerated until its use.

For HA/COL ink production, ALG/HA ink (30:70), without adding the crosslinker was kept at 10 °C for 24 hours. Afterwards, 1.8 g of COL in 10 mL of 0.02 M acetic acid (10 °C) was added to the ALG/HA solution and 10 mL of acetic acid was added. Due to its high viscosity, the HA/COL ink does not require primary crosslinking. The ink was mixed to avoid clogging the nozzle during filament extrusion. Subsequently, the ink was kept refrigerated until its use.

Manufacturing of 3D printed scaffolds

The 3D printed HA/COL and HA scaffolds were fabricated using the Octopus™ 3D Biotechnologies Solutions (3DBS – Campinas, Brazil) bioprinter. The scaffold design and slicing were performed using PrusaSlicer® software version 2.4.0. The scaffold geometry consisted of a cylindrical shape with dimensions of 25 x 25 x 5 mm (Figure 1). The syringe was filled with ink and subjected to gentle tapping to remove air bubbles.

Other parameters such as layer height, print speed, and fill orientation (Table 1) were determined after repetitions to ensure consistency and reproducibility. At the end of the printing process, the 3D printed HA scaffolds underwent a secondary crosslinking in a 10% $CaCl_2$ solution for 20 minutes, while the 3d printed HA/COL scaffolds underwent a primary crosslinking at the same concentration and duration. After, the scaffolds were thoroughly washed with distilled water to remove the crosslinking agent. The scaffolds were dried at room temperature for contraction of size, followed by drying in an oven at 37 °C to remove residual moisture.

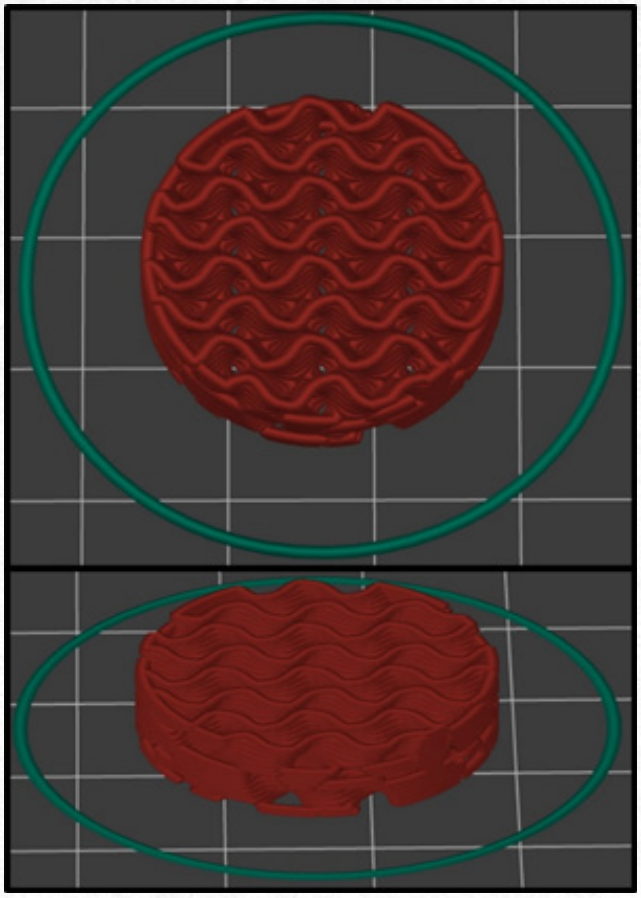

Figure 1 - 3D model used for manufacturing HA and HA/COL scaffolds.

Parameters	
Scaffold fill	40%
Filling orientation	45°
Layer height	0.3 mm
Print speed	3 mm/s
Speed of unprinted movements	60 mm/s
Extrusion thickness	1 mm
Tip diameter	0.5 mm

Table 1 - 3D printing parameters.

Characterization of 3D printed scaffolds

Yield of collagen

At the end of collagen processing, the yield of lyophilized collagen was calculated using the following equation 1 [41]:

$$\text{Yield (\%)} = \frac{M}{M_0} \times 100\% \quad (1)$$

Where M_0 is the mass of the tilapia skin lyophilized before pretreatment and M is the mass of the lyophilized collagen.

Scanning Electron Microscopy (SEM) and macroscopic images

The 3D printed HA and HA/COL scaffolds were gold-coated for morphological analysis using SEM equipment (LEO, Model: 440) operated at 15 kV and a magnification of 100x and 1000x. The images were obtained at the Institute of Chemistry of São Carlos (IQSC-USP).

Energy Dispersive X-Ray Spectroscopy (EDS)

The elemental content and the Ca/P ratio determination of the 3D printed HA and HA/COL scaffolds were investigated by Energy Dispersive X-ray Spectrometry (EDS). The analyses were carried out at the Tribology and Composites Laboratory (LTC) of the School of Engineering of São Carlos (EESC) - USP.

Fourier Transform Infrared Spectroscopy (FT-IR)

The FT-IR spectrometer (Shimadzu Prestige-21) was used to identify the functional groups present in the COL, ALG, and HA powders. The powders were mixed with KBr at a ratio of 1:100 and pressed to form pellets. The spectral range will be measured between 4000 and 400 cm^{-1}, with a resolution of 2 cm^{-1}.

X-Ray Diffraction (XRD)

To confirm the crystalline phase composition, an X-ray diffractometer (Shimadzu XDR-7000) was used with 40 kV and 30 mA radiation, CuK-α (wavelength λ = 1.54056 Å). Spectra were recorded from θ = 2θ = 10° to 80° with a step size of 0.02° every 0.6 s. Hydroxyapatite was used as a reference and compared to standard hydroxyapatite (COD 9013627) and monetite (COD 210684) obtained in .cif format from the Crystallography Open Database (COD). The analysis was performed at the Tribology and Composites Laboratory (LTC) of the School of Engineering of São Carlos (EESC) - USP. The crystallinity index of the scaffolds was evaluated according to equation 2.

$$Xc = \frac{\text{area of all crystalline peaks}}{\text{area of all crystalline and amorphous peaks}} \quad (2)$$

Porosity

The volumetric percentage porosity of the scaffolds (n=5) was measured according to the Archimedes principle [42]. The porosity was calculated using equation 3

$$\text{Porosity (\%)} = \frac{W2-W1}{W2-W3} \times 100\% \quad (3)$$

Where W1 is the dry weight of the scaffold, W2 is the wet weight of the scaffold (including ethanol solution at a temperature below room temperature to avoid evaporation), and W3 is the weight of the scaffold in 99.5% ethanol solution (subtracting the buoyancy of W1).

Swelling ratio

The water absorption capacity was analyzed by the degree of swelling of the samples according to the method performed by Ahmadian et al.[43]. The scaffolds (n=5) were weighed and immersed in 20 mL of water (pH=7.3) in 50 mL falcon tubes and incubated at 37 °C. After 1, 3, 18, 24, 48, and 72 hours, the scaffolds were removed and dried with filter papers. The weight of the swollen scaffolds will be measured using an analytical balance. The degree of swelling of the scaffolds will be obtained according to equation 4:

$$\text{Swelling ratio} = \frac{Ws-Wd}{Wd} \quad (4)$$

Where Ws and Wd represent the weight of the swollen and dried scaffolds, respectively.

pH evaluation

The pH of the incubation medium was measured using a pH meter (Orion Star A211, Thermo Scientific, Massachusetts, USA). A curve was obtained for the pH data after incubation periods of 1, 3, 7, 14, and 21 days.

In vitro assay

Cell lineages

In this study, the osteoblast-like cell line known as MC3T3-E1 was used. The cells were cultivated in flasks using Minimum Essential Medium alpha (MEM-α) supplemented with 10% Fetal Bovine Serum (FBS). The cultivation was carried out at a temperature of 37 °C in a humid atmosphere with 5% CO2. To ensure optimal growth conditions, the cells were maintained at densities below the confluence and passaged every 2-3 days until they were ready for experimentation.

MTT

The cells were seeded into a 24-well culture plate at a concentration of 1x104 cells per well for a period of 1, 3, and 7 days. This assay was performed by placing the scaffolds in contact with the cells. At the end of the experimental period, each well of the culture plate was washed with Phosphate-Buffered Saline (PBS), and 250 µL of MTT solution (0.5 mg/mL) (Sigma - Aldrich Corp®, St. Louis, MO, United States) was added. The cells were incubated (5% CO2, 37°C) for 3 hours. After the incubation period, 500 µL of isopropanol was added to each well to dissolve the formazan crystals, and the absorbance at 590 nm was measured using a microplate reader (Bio-Tek Instruments).

Statistical analysis

All data obtained in the study were analyzed in the form of means and standard deviations. Initially, the distribution of variables was tested using the Shapiro-Wilk normality test. The analyzed variables exhibited a normal distribution, and comparisons between groups were performed using analysis of variance (ANOVA), followed by Tukey's post-hoc test. The statistical software used was GraphPad Prism version 9.0, and the adopted significance level was 5% ($p \leq 0.05$).

Results

Collagen yield

The collagen yield obtained by acid extraction was 41.895%. The wet mass of collagen obtained after the removal of scales and skin was 84.08 g. After lyophilization, the mass of tilapia skin was 27.15 g, considered as the initial mass for yield calculation. Then, the lyophilized skin underwent pre-treatment and lyophilization, resulting in a mass of 24.289 g. At the end of the purification, freezing, and lyophilization steps of the obtained collagen, the sum of the masses resulted in 11.3745 g.

Sem and macroscopic images

SEM morphology of the 3D printed HA and HA/COL scaffolds is shown in Figure 2. Figure 2A illustrates the macroscopic overview of 3D printed HA scaffolds, demonstrating an approximate size of 16 mm post-drying. In Figure 2B, SEM image at 500x magnification reveals a homogeneous structure in the 3D printed HA scaffold, with well-defined interconnected macropores fabricated through the 3D printing process. Figure 2C demonstrates the effective integration of two materials, ALG and HA, forming a porous network while maintaining distinct particles of each material.

Furthermore, in Figure 2D it is possible to observe that 3D printed HA/COL scaffolds had a size of approximately 14 mm after drying. Figure 2E presents the scanning SEM image (500x) of the 3D printed HA/COL scaffold. Notably, the structure exhibits a more fibrous appearance, though it remains homogeneous. Additionally, interconnected macropores, formed through the 3D printing process, are evident. In Figure 2F, the incorporation of COL is evident, featuring apparent fibers into the particulate structure.

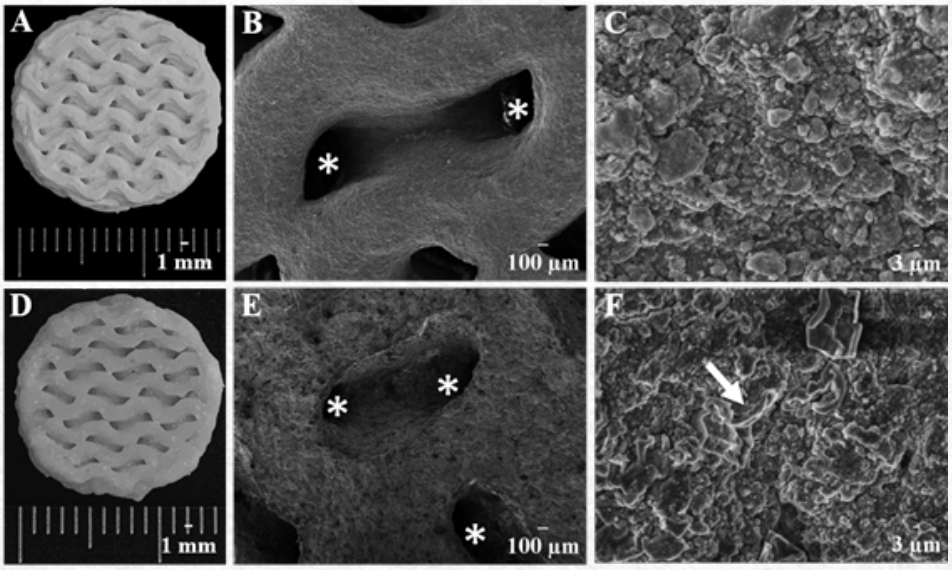

Figure 2- Macroscopic and SEM images of HA and HA/COL scaffolds. (A) Macroscopic image of HA scaffold (B) SEM microphotography of HA scaffold in a magnitude of 500x (C) SEM microphotography of HA scaffold in a magnitude of 1000x (D) Macroscopic image of HA/COL scaffold (E) SEM microphotography of HA/COL in a magnitude of 500x (F) SEM microphotography of HA/COL in a magnitude of 1000x. (* indicates the pores, ➞ indicates the COL fiber).

EDS

The EDS analysis results are shown in Table 2. In the 3D printed HA scaffold, a significant abundance of calcium (Ca) and phosphate (P) elements was observed, consisting of 52.726% and 34.898%, respectively. Also, the elements chlorine (Cl), silica (Si), potassium (K), strontium (Sr), and palladium (Pd) were identified, consisting of 10.022%, 2.004%, 0.189%, 0.159% and 0.002%, respectively. Moreover, in the 3D printed HA/COL scaffold, the elements Ca, P, Cl, Si, K, and Sr were obtained with percentages of 51.995%, 22.214%, 21.936%, 0.781%, 0.359%, and 0.243%, respectively. The element Pd was not detected; nonetheless, the elements sodium (Na) and sulfur (S) were identified at percentages of 2.100% and 0.413%, respectively. In addition, the Ca/P ratio of the 3D printed HA and HA/COL scaffolds were 1.510 and 2.340, respectively.

Element	Content of Elements by Weight (%)	
	HA	HA/COL
Ca	52.726	51.995
P	34.898	22.214
Cl	10.022	21.936
Si	2.004	0.781
K	0.189	0.359
Sr	0.159	0.243
Pd	0.002	-
Na	-	2.100
S	-	0.413

Table 2- EDS spectrum results of elements observed in HA and HA/COL scaffolds. The percentage was calculated from qualitative analyses of the atomic mass of each element, which results in a % of element mass.

Other parameters such as layer height, print speed, and fill orientation (Table 1) were determined after repetitions to ensure consistency and reproducibility. At the end of the printing process, the 3D printed HA scaffolds underwent a secondary crosslinking in a 10% $CaCl_2$ solution for 20 minutes, while the 3d printed HA/COL scaffolds underwent a primary crosslinking at the same concentration and duration. After, the scaffolds were thoroughly washed with distilled water to remove the crosslinking agent. The scaffolds were dried at room temperature for contraction of size, followed by drying in an oven at 37 °C to remove residual moisture.

Figure 3A illustrates the FTIR spectrum, demonstrating ALG peaks consistent with O-H

Moreover, in Figure 3B, the FTIR spectrum of the HA scaffold exhibits peaks from 3575 cm^{-1} to 3325 cm^{-1}, indicative of O-H stretching, a peak at 1620 cm^{-1} corresponds to C=O stretching, while a -COOH an in-plane bending appears at 1433 cm^{-1}. Furthermore, a C-O-C stretching at 1030 cm^{-1} is observed, with the PO_4^{3-} v3 stretching antisymmetric and PO_4^{3-} v4 bending, with Ca-O stretching ranging from 550 cm^{-1} to 600 cm^{-1}. Likewise, the FTIR spectrum of HA/COL scaffolds presents peaks of O-H stretching and Amide A in the range of 3575 cm^{-1} to 3325 cm^{-1}, a C=O stretching and Amide I peaks occur within the 1620 cm^{-1} to 1640 cm^{-1} range, -COOH peak is apparent at 1433 cm^{-1}, while an Amide III peak is at 1244 cm^{-1}. Additionally, a C-O-C stretching at 1030 cm^{-1} is observed with PO_4^{3-} v3 antisymmetric pattern stretching and PO_4^{3-} v4 bending with Ca-O stretching within the range of 550 cm^{-1} to 600 cm^{-1}.

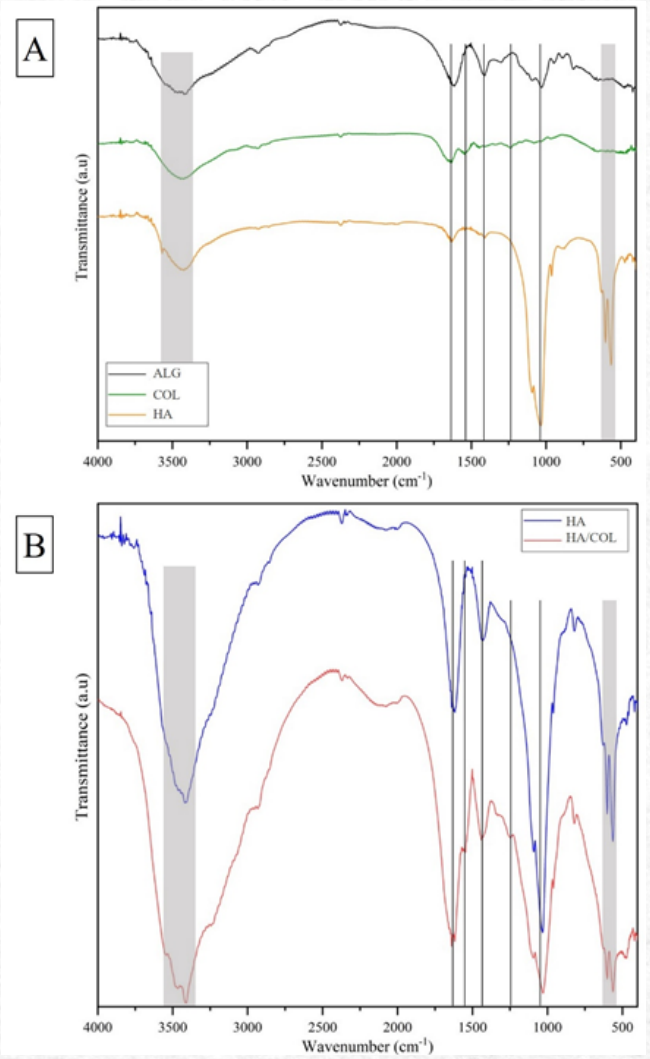

Figure 3- FTIR spectrum peak results. (A) Elements observed in raw materials ALG, HA and COL (B) Elements observed in 3D printed HA and HA/COL scaffolds.

X-Ray Diffraction (XRD)

The XRD patterns of HA powder are shown in Figure 4. From the diffraction peaks, it was observed that the HA presented two crystalline phases of calcium phosphates: HA and monetite (DCPA). The main diffraction peaks are found at 10.85°, 25.83°, 31.73°, 32.88°, and 39.81° in 2θ (°) and correspond to the planes (100), (002), (211), (300), and (311) for HA, respectively. The XRD peak located at 30.30° in 2θ (°) corresponds to the monetite phase.

The crystallinity index (Xc) for the CaP phases was measured from the X-ray diffraction pattern by calculating and summing the area of each significant peak by the total area. According to equation, the obtained crystallinity index was Xc = 72.26%.

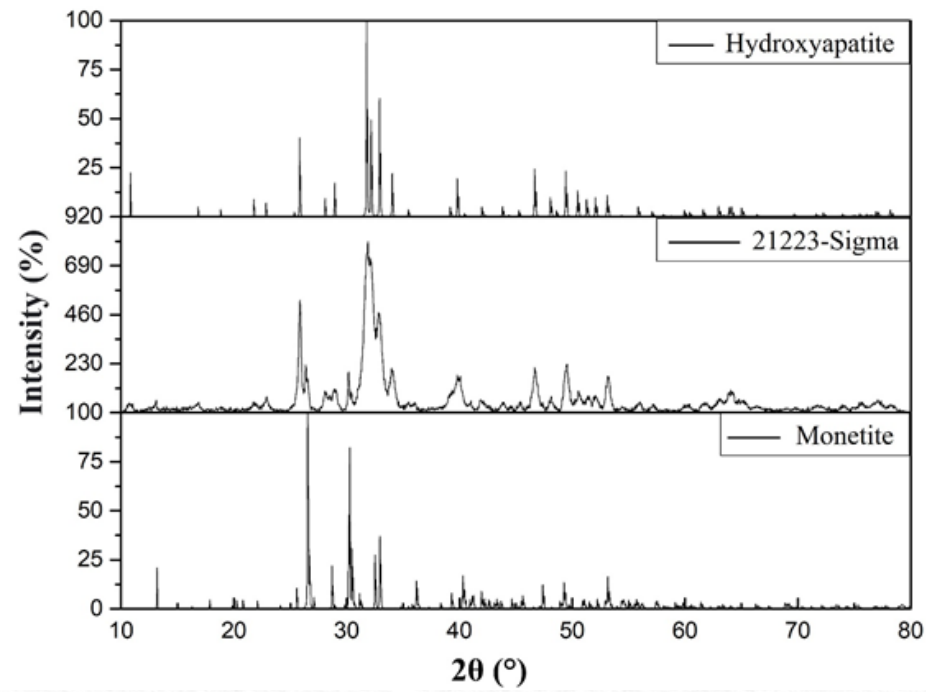

Figure 4- X-ray diffractograms of the HA powder sample (#21223) and the hydroxyapatite and monetite standards.

Porosity

Figure 5 demonstrates the values found for porosity evaluation. It is possible to observe that 3D printed HA scaffolds presented a mean porosity of 36.9 % ± 4.4 and 3D printed HA/COL scaffolds of 29.9 % ± 4.2. Statistical analysis demonstrated that 3D printed HA scaffolds presented higher values compared to 3D printed HA/COL scaffolds ($p<0.05$) (Figure 5).

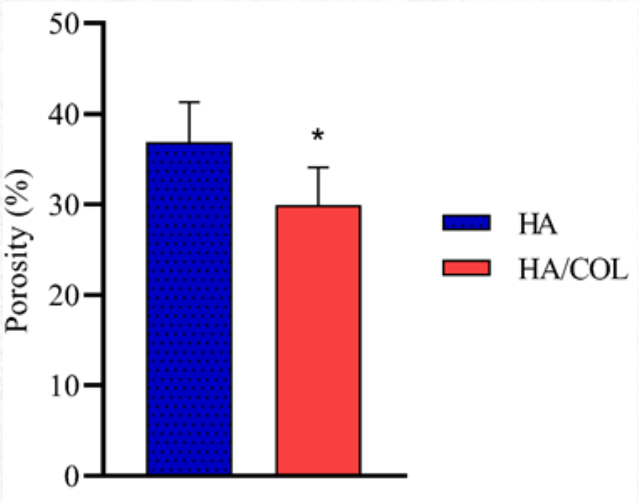

Figure 5- Results of porosity for HA and HA/COL scaffolds (results are expressed as the mean ± SD for 3 replicates, n = 5). ANOVA and post-hoc de Tukey ($p < 0.05$): *$p < 0.05$.

Swelling ratio

The swelling ratio for 3D printed HA scaffolds were 34.632%, 36.816%, 35.182%, 43.119%, 39.924%, and 39.887% after immersion for 1, 3, 18, 24, 48, and 72 hours, respectively. For the 3D printed HA/COL scaffolds, the swelling ratio is 54.816% (1 h), 51.149% (3 h), 37.231% (18 h), 37.898% (24 h), 36.644% (48 h), and 22.612% (72 h). Statistical analysis demonstrated that 3D printed HA scaffolds presented lower values compared to 3D printed HA/COL at 1 and 3 hours ($p<0.05$). Otherwise, 3D printed HA scaffolds presented higher values compared to 3D printed HA/COL scaffolds at day 72 hours ($p<0.05$) There was no other statistical difference (Figure 6).

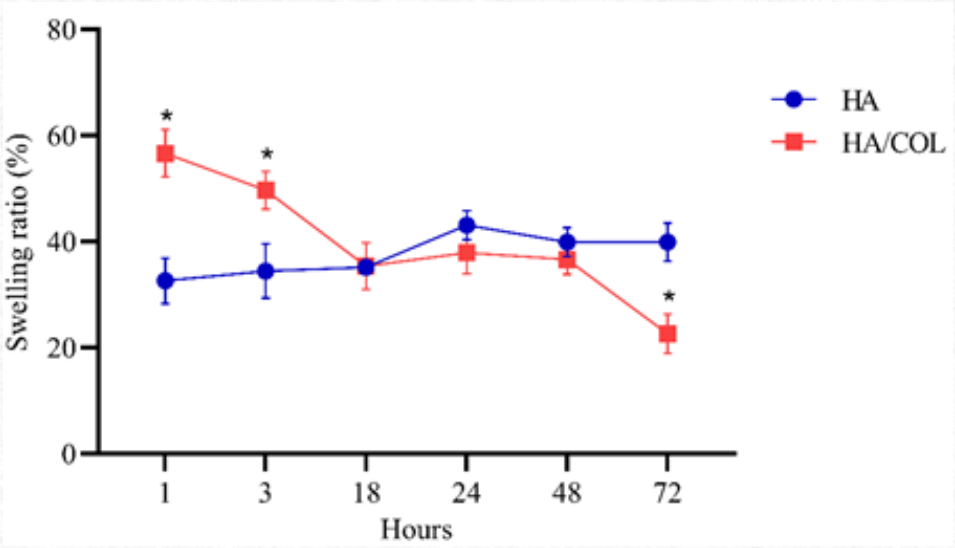

Figure 6- Results of swelling ratio for HA and HA/COL scaffolds (results are expressed as the mean ± SD for 3 replicates, n = 5). ANOVA and post-hoc de Tukey ($p < 0.05$): *$p < 0.05$.

Mass loss

Figure 7 shows the mass loss rate of 3D printed HA and HA/COL scaffolds over an experimental period of 1, 3, 7, 14, and 21 days. The variation in mass loss of the 3D printed HA scaffolds ranged from 69.70 to 82.02 and for 3D printed HA/COL scaffolds ranged from 92.67 to 97.72. At all experimental times, 3D printed HA scaffolds showed higher values with significant differences compared to 3D printed HA/COL scaffolds ($p<0.05$).

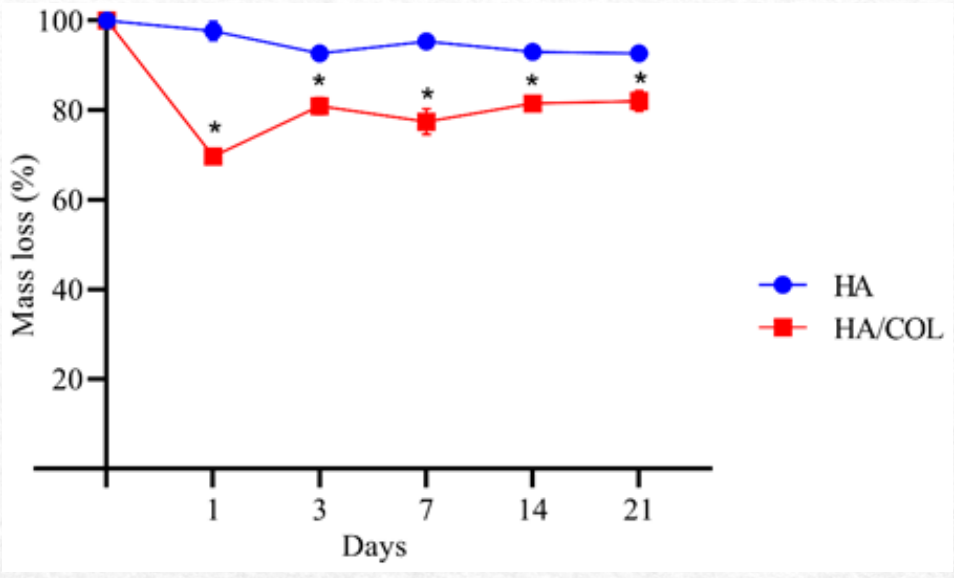

Figure 7- Evaluation of mass loss of HA and HA/COL scaffolds (results are expressed as the mean ± SD for 3 replicates, n = 5). ANOVA and post-hoc de Tukey ($p < 0.05$): *$p < 0.05$.

pH evaluation

Figure 8 shows the pH variation of the PBS solution (initially 7.4) over an experimental period of 1, 3, 7, 14, and 21 days. The pH measured on days 1, 3, 7, 14, and 21 days for the 3D printed HA scaffold was 7.038, 6.978, 6.885, 6.866, and 6.822, respectively. The pH of the 3D printed HA scaffolds gradually decreased over time, from 7.038 on day 1 to 6.822 on day 21. The pH measured on days of 1, 3, 7, 14, and 21 days for 3D printed HA/COL scaffolds was 7.056, 6.890, 6.768, 6.870, and 6.812, respectively. The 3D printed HA/COL scaffolds reached their lowest pH on the day 7 and showed a significant difference compared to 3D printed HA scaffolds ($p<0.05$).

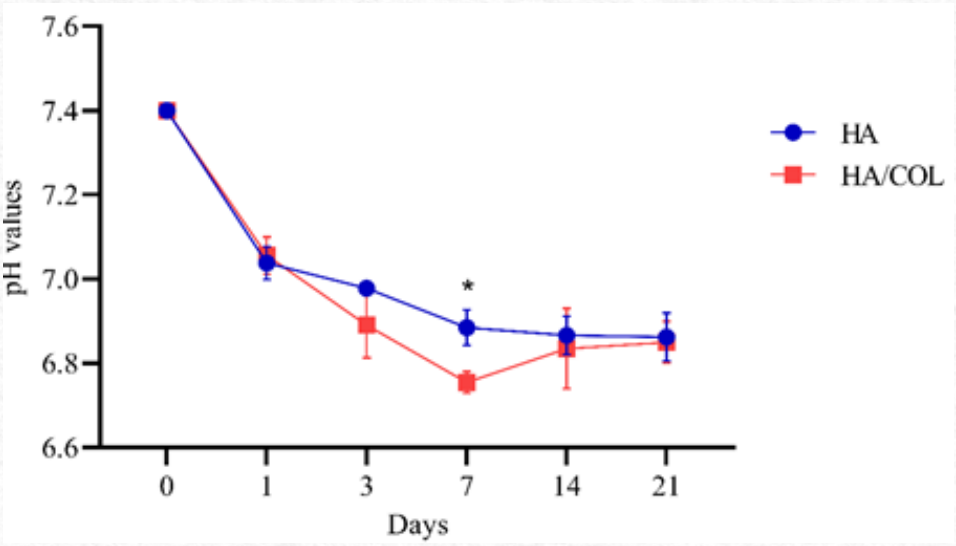

Figure 8- Results of pH evaluation for HA and HA/COL scaffolds (results are expressed as the mean ± SD for 3 replicates, n = 5). ANOVA and post-hoc de Tukey ($p < 0.05$): *$p < 0.05$.

MTT

The results of MTT for the MC3T3-E1 cell line are shown in Figure 9. On day 1, CG presented higher cell viability values compared to 3D printed HA and HA/COL scaffolds. On days 3 and 7 there were no significant differences ($p<0.05$). At all experimental times, cell proliferation above 70% was noted compared to CG.

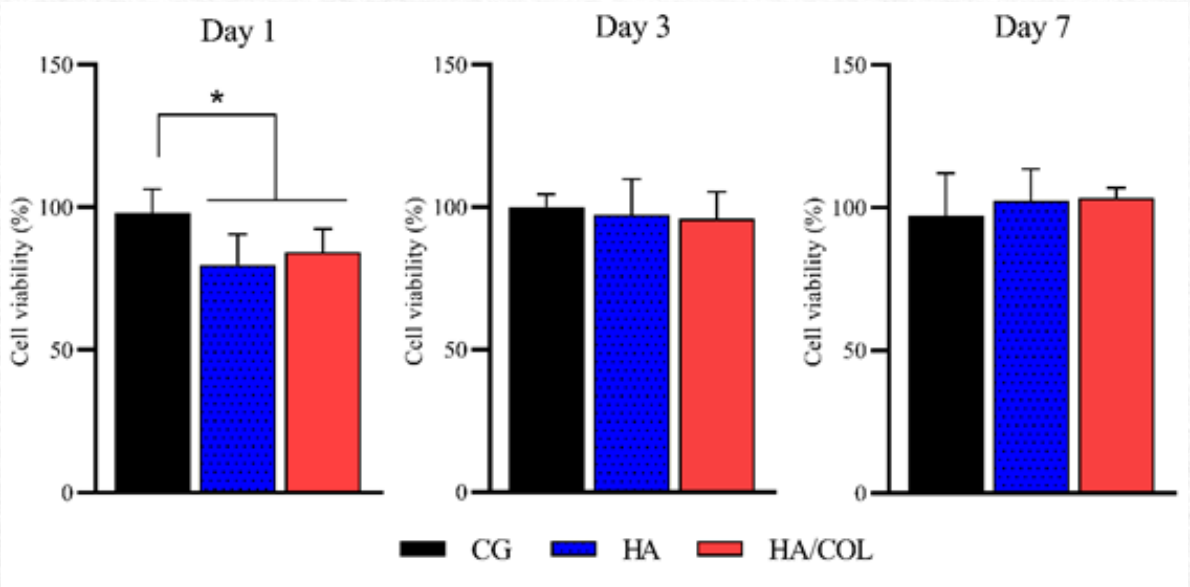

Figure 9- Results of proliferative activity by MTT of MC3T3-E1 cell line in the experimental periods (results are expressed as the mean ± SD for 3 replicates, n = 5). ANOVA and post-hoc de Tukey ($p < 0.05$): *$p < 0.05$.

Discussion

The present study investigated the physicochemical characteristics and biological effects of 3D printed HA scaffolds and 3D printed HA enriched with Col extracted from fish skin (tilapia). SEM analysis demonstrated the particulate aspect of HA and the fibrous of COL and that both materials were well mixed into the scaffolds. Moreover, a higher Ca/P ratio was observed for 3D printed HA/COL scaffolds and FTIR demonstrated peaks of O-H, Amide A, C-O-C and Ca-O. For 3D printed HA/COL scaffolds, the porosity was lower, the mass loss was higher and the hydration ratio was higher 1 hour after immersion but decreased after 72 hours. pH values were similar after 21 days of immersion. The in vitro studies demonstrated that the materials have not present any cytotoxicity (cell proliferation for all experimental periods was above 70% for both treated groups).

The inclusion of COL into HA is a promising strategy for bone tissue engineering due to the well-known capacity of improving the biological properties and accelerating the degradation of ceramic materials [8]. These characteristics are crucial to the successful performance of the materials, since the degradation rate of a biomaterial can influence cell growth, tissue regeneration, and host response[44,45].

The COL yield for the fish samples was of 41.89%. This rate is very discrepant among the studies and can be attributed to the protocol of extraction used and to the variations in the distribution of alignment and composition of the fish matrices[46]. For example, Chen et al.[47] reported a COL yield of 27.7% using the acidic extraction of tilapia (Oreochromis niloticus) skin. Additionally, Veeruraj et al.[48] found an 80% collagen yield through acidic extraction from the skin of eel fish (Evenchelys macrura).

Furthermore, SEM results reveal notable differences in the scaffold structures. Specifically, in 3D printed HA scaffolds, the absence of visible ALG fibers is observed, demonstrating a homogeneous structure despite the potential observation of particulate arrangement. This absence, however, is attributed to the successful integration of HA into the ALG fibers, allowing for scaffold printing without compromising the shape of the filament. The same structure was seen in the work of Iglesias-Mejuto and García-González[49], where alginate and HA scaffolds demonstrated a homogeneous structure. The 3D printed HA/COL scaffolds exhibit a rougher structure compared with 3D printed HA scaffolds, by integrating COL fibers into the structure of HA and ALG, this result corroborates with the findings of Pati et al[50], where fish COL scaffolds exhibited a fibrous architecture.

Moreover, SEM findings are further substantiated by FTIR analysis, which identifies characteristic peaks corresponding to ALG, HA, and COL. These peaks serve as evidence for the accurate preparation of the ink, highlighting the preservation of molecular characteristics during the printing process. Similarly, Han et al.[51] demonstrated that the AG peaks correspond to hydroxyl (–OH), carbonyl (C=O), and carboxyl (COOH), and also that the HA peaks correspond to hydroxyl vibrations and phosphate stretching vibrations. The findings of COL, on the other hand, corroborate with the work of Slimane and Sadok[52], where peaks of Amide A, Amide I, Amide II, and Amide III were also identified in a sample of collagen from cartilaginous fish (Mustelus mustelus).

Thus, the Ca/P ratio of the scaffolds, assessed by EDS, approaches the stoichiometric value of HA (~1.67). This data corroborates with the range observed in human bone, where the Ca/P ratio typically varies from 1.37 to 1.87[53]. The accentuated value for the HA structures occurred due to crosslinking with 10% $CaCl_2$. Another significant finding is the detection of residual Na in the 3D printed HA/COL scaffold sample at 2.100%, which is related to the NaCl used in the tilapia skin pretreatment process.

Furthermore, the porosity of the scaffolds is related to their manufacturing process and the properties of the materials involved. COL, being a fibrous protein, can occupy pores in HA scaffolds, as evidenced by SEM images where the pores in 3D printed HA scaffolds are larger and better defined than in 3D printed HA/COL scaffolds. Thus, scaffold pore size and connectivity are critical points to be considered, once they are related to an adequate vascularization and cell attraction [54]. Research findings indicate that porous HA scaffolds can notably enhance the adhesion, proliferation, and migration of mesenchymal stem cells derived from rat bone marrow facilitate the ingrowth of new bone, and promote neovascularization in the region of the bone defect[55].

Moreover, the swelling ratio for 3D printed HA scaffolds ranged from 34% to 44%, while the swelling ratio for 3D printed HA/COL scaffolds varied between 22% and 55%. Furthermore, the rapid hydration of 3D printed HA/COL scaffolds is attributed to the high liquid absorption capacity of COL, which may be associated with the presence of hydrophilic functional groups such as NH_2 and COO^- in the biopolymers [56]. However, this capacity gradually decreases over time, suggesting possible degradation of the organic part of the scaffold. Homogeneity during the periods studied in hydration for scaffolds produced with HA is associated with the degree of crosslinking and the incorporation of inorganic particles, such as HA structures.

The mass loss of the 3D printed HA/COL scaffolds was significantly lower compared to 3D printed HA scaffolds.

It is known that the rate of HA dissolution is low, which may be a disadvantage of using this material as bone graft [57,58]. For bone ingrowth, resorption of the bone substitute material is mandatory since the formation of newly formed bone in the defect area needs the liberation of space[59–61]. Thus, it seems that the introduction of COL into HA constituted a potential strategy, allowing the acceleration of the material degradation (demonstrated by the higher mass loss), which consequently, could stimulate the substitution of the material for new bone. These findings corroborate those of Parisi *et al*.[62] who also observed a mass loss of scaffolds manufactured with HA and collagen from marine sponges.

The analysis of the pH demonstrated a decrease of the values during the experimental periods for both scaffolds with no difference among them being all the values around the physiological. Also, this behavior constitutes a positive aspect of the use of HA and HA associated to COL for bone tissue engineering purposes. Values of pH around 7.4 produced a more homeostatic environment which may have a positive influence in cell metabolism and tissue regeneration [63,64]. As the degradation of HA is slow, there is no immediate release of ions to the medium with no alkalinization or acidification of the medium. Interestingly, the addition of COL also had no effect on pH values. Magri *et al.*[65] and Parisi *et al*.[62] also showed that the incorporation of Col in Bioglass and HA -based materials had no effect in the pH measurements, with values close to the physiological one. Additionally, the in vitro studies demonstrated that 3D printed scaffolds had a positive effect on the viability of osteoblast cells (with a minimum of 70% viability rate). Likewise, Eshkol-Yogev *et al.*[66] found an increase of osteoblast proliferation cultured in the presence of HA hydrogels. The osteoconductive properties of HA is well known but this material presents no osteoinductive activity (limiting its osteogenic potential and its use in the clinical setting) [67]. Thus, COL introduction may play an important role in the improvement of the biological performance of HA, increasing bone mineralization and tissue ingrowth [67]. The association of HA and COL has been used to improve osteoblast differentiation[68]. The in vitro results of the present study demonstrated that COL can be used as the organic part of a bone bioinspired graft, mimicking better the composition of the human bone tissue[69], possibly constituting a bone graft with improved biological properties.

Fish COL has been emerging as promising source of COL once it is biocompatible, easy to obtain, and presents osteogenic properties[70]. Each year, over 20 million tons of fish by-products—such as fins, heads, skin, and viscera—are discarded, representing a valuable and sustainable raw material for collagen extraction[71]. Moreover, the combination of proteins like fish Col with HA enables the development of biomaterials with enhanced mechanical properties, including improved strength, elongation, toughness, and controlled degradation[72]. Furthermore, these composites exhibit greater bioactivity and biocompatibility, contributing to a better understanding of biomineralization processes [33]. In this context, our results demonstrated that the incorporation of COL into HA was possible and produced an improvement in the physical-chemical characteristics and in the biological performance of the 3D scaffolds. The material percentage was used to design a bio-inspired composite, mimicking the composition of bone tissue and possibly being a more effective bone substitute[73–75]. In this context, 3D printed HA/COL scaffolds might constitute a more appropriated structure for bone regeneration compared to HA only.

Conclusion

Based on our investigations of 3D printed HA/COL scaffolds were successfully obtained with improved biological properties, especially the one mimicking the composition of bone (with 70% of HA and 30% of COL). Consequently, these data highlight the potential of the introduction of COL into HA to improve the performance of the graft for bone regeneration applications. Further long-term studies should be carried out to provide additional information concerning the late stages of material degradation and bone healing by the HA/COL.

References

1. Panteli M, Pountos I, Jones E, Giannoudis P V. Biological and molecular profile of fracture non-union tissue: current insights. J Cell Mol Med. 2015 Apr;19(4):685–713.
2. Calori GM, Albisetti W, Agus A, Iori S, Tagliabue L. Risk factors contributing to fracture non-unions. Injury. 2007 May;38 Suppl 2:S11-8.
3. Edderkaoui B. Potential Role of Chemokines in Fracture Repair. Front Endocrinol (Lausanne). 2017;8:39.
4. Marew T, Birhanu G. Three dimensional printed nanostructure biomaterials for bone tissue engineering. Regen Ther. 2021 Dec;18:102–11.
5. Battafarano G, Rossi M, De Martino V, Marampon F, Borro L, Secinaro A, et al. Strategies for Bone Regeneration: From Graft to Tissue Engineering. Int J Mol Sci. 2021 Jan;22(3).
6. Al-Shalawi FD, Mohamed Ariff AH, Jung DW,

Mohd Ariffin MK, Seng Kim CL, Brabazon D, et al. Biomaterials as Implants in the Orthopedic Field for Regenerative Medicine: Metal versus Synthetic Polymers. Vol. 15, Polymers. 2023.

7. Yu X, Tang X, Gohil S V, Laurencin CT. Biomaterials for Bone Regenerative Engineering. Adv Healthc Mater. 2015 Jun;4(9):1268–85.
8. Ielo I, Calabrese G, De Luca G, Conoci S. Recent Advances in Hydroxyapatite-Based Biocomposites for Bone Tissue Regeneration in Orthopedics. Int J Mol Sci. 2022 Aug;23(17).
9. Ige OO, Umoru LE, Aribo S. Natural Products: A Minefield of Biomaterials. Burkel E, editor. ISRN Mater Sci. 2012;2012:983062.
10. Yamamura H, da Silva VHP, Ruiz PLM, Ussui V, Lazar DRR, Renno ACM, et al. Physico-chemical characterization and biocompatibility of hydroxyapatite derived from fish waste. J Mech Behav Biomed Mater. 2018 Apr 1;80:137–42.
11. de Moura NK, Siqueira IAWB, Machado JP de B, Kido HW, Avanzi IR, Rennó ACM, et al. Production and characterization of porous polymeric membranes of pla/pcl blends with the addition of hydroxyapatite. J Compos Sci. 2019;3(2).
12. Lei X, Gao J, Xing F, Zhang Y, Ma Y, Zhang G. Comparative evaluation of the physicochemical properties of nano-hydroxyapatite/collagen and natural bone ceramic/collagen scaffolds and their osteogenesis-promoting effect on MC3T3-E1 cells. Regen Biomater. 2019 Dec;6(6):361–71.
13. Montalbano G, Molino G, Fiorilli S, Vitale-Brovarone C. Synthesis and incorporation of rod-like nano-hydroxyapatite into type I collagen matrix: A hybrid formulation for 3D printing of bone scaffolds. J Eur Ceram Soc. 2020;40(11):3689–97.
14. De Lama-Odría MDC, Valle LJ Del, Puiggalí J. Lanthanides-Substituted Hydroxyapatite for Biomedical Applications. Int J Mol Sci. 2023 Feb;24(4).
15. Pang KM, Lee JK, Seo YK, Kim SM, Kim MJ, Lee JH. Biologic properties of nano-hydroxyapatite: An in vivo study of calvarial defects, ectopic bone formation and bone implantation. Biomed Mater Eng. 2015;25(1):25–38.
16. Siddiqui HA, Pickering KL, Mucalo MR. A Review on the Use of Hydroxyapatite-Carbonaceous Structure Composites in Bone Replacement Materials for Strengthening Purposes. Mater (Basel, Switzerland). 2018 Sep;11(10).
17. Wang H. A Review of the Effects of Collagen Treatment in Clinical Studies. Polymers (Basel). 2021 Nov;13(22).
18. Niu Y, Stadler FJ, Yang X, Deng F, Liu G, Xia H. HA-coated collagen nanofibers for urethral regeneration via in situ polarization of M2 macrophages. J Nanobiotechnology. 2021 Sep;19(1):283.
19. Yu L, Wei M. Biomineralization of collagen-based materials for hard tissue repair. Int J Mol Sci. 2021;22(2):1–17.
20. Santana A de F, Avanzi IR, Parisi JR, Cruz MA, Do Vale GCA, de Araújo TAT, et al. In vitro and in vivo genotoxicity and cytotoxicity analysis of protein extract from aplysina fulva sponges. Acta Sci - Biol Sci. 2021;43:1–13.
21. Fernandes KR, Parisi JR, de Almeida Cruz M, Gabbai-Armelin PR, de Araújo TAT, de França Santana A, et al. Characterization and Biological Performance of Marine Sponge Collagen. Brazilian Arch Biol Technol. 2021;64.
22. Chen S, Hirota N, Okuda M, Takeguchi M, Kobayashi H, Hanagata N, et al. Microstructures and rheological properties of tilapia fish-scale collagen hydrogels with aligned fibrils fabricated under magnetic fields. Acta Biomater. 2011 Feb;7(2):644–52.
23. Govindharaj M, Roopavath UK, Rath SN. Valorization of discarded Marine Eel fish skin for collagen extraction as a 3D printable blue biomaterial for tissue engineering. J Clean Prod. 2019;230:412–9.
24. Qin D, Bi S, You X, Wang M, Cong X, Yuan C, et al. Development and application of fish scale wastes as versatile natural biomaterials. Chem Eng J. 2022;428:131102.
25. Ali AMM, Benjakul S, Prodpran T, Kishimura H. Extraction and Characterisation of Collagen from the Skin of Golden Carp (Probarbus Jullieni), a Processing By-Product. Waste and Biomass Valorization. 2018;9(5):783–91.
26. Nagai T, Suzuki N. Isolation of collagen from fish waste material — skin, bone and fins. Food Chem. 2000;68(3):277–81.
27. Yu D, Chi CF, Wang B, Ding GF, Li ZR. Characterization of acid-and pepsin-soluble collagens from spines and skulls of skipjack tuna (Katsuwonus pelamis). Chin J Nat Med. 2014 Sep;12(9):712–20.
28. Hu Z, Yang P, Zhou C, Li S, Hong P. Marine collagen peptides from the skin of Nile Tilapia

(Oreochromis niloticus): Characterization and wound healing evaluation. Mar Drugs. 2017;15(4):102.

29. Lau CS, Hassanbhai A, Wen F, Wang D, Chanchareonsook N, Goh BT, et al. Evaluation of decellularized tilapia skin as a tissue engineering scaffold. J Tissue Eng Regen Med. 2019 Oct;13(10):1779–91.

30. Lim YS, Ok YJ, Hwang SY, Kwak JY, Yoon S. Marine Collagen as A Promising Biomaterial for Biomedical Applications. Vol. 17, Marine Drugs. 2019. p. 467.

31. Venkatesan J, Kim SK. Nano-hydroxyapatite composite biomaterials for bone tissue engineering--a review. J Biomed Nanotechnol. 2014 Oct;10(10):3124–40.

32. Schuster L, Ardjomandi N, Munz M, Umrath F, Klein C, Rupp F, et al. Establishment of Collagen: Hydroxyapatite/BMP-2 Mimetic Peptide Composites. Mater (Basel, Switzerland). 2020 Mar;13(5).

33. Kavitha Sri A, Arthi C, Neya NR, Hikku GS. Nano-hydroxyapatite/collagen composite as scaffold material for bone regeneration. Biomed Mater. 2023 Apr;18(3).

34. Chen XB, Fazel Anvari-Yazdi A, Duan X, Zimmerling A, Gharraei R, Sharma NK, et al. Biomaterials / bioinks and extrusion bioprinting. Bioact Mater. 2023;28:511–36.

35. Feng Y, Zhu S, Mei D, Li J, Zhang J, Yang S, et al. Application of 3D Printing Technology in Bone Tissue Engineering: A Review. Vol. 18, Current Drug Delivery. 2021. p. 847–61.

36. Bisht B, Hope A, Mukherjee A, Paul MK. Advances in the Fabrication of Scaffold and 3D Printing of Biomimetic Bone Graft. Ann Biomed Eng. 2021 Apr;49(4):1128–50.

37. Ardelean IL, Gudovan D, Ficai D, Ficai A, Andronescu E, Albu-Kaya MG, et al. Collagen/hydroxyapatite bone grafts manufactured by homogeneous/heterogeneous 3D printing. Mater Lett. 2018;231:179–82.

38. Dong Q, Zhang M, Zhou X, Shao Y, Li J, Wang L, et al. 3D-printed Mg-incorporated PCL-based scaffolds: A promising approach for bone healing. Mater Sci Eng C Mater Biol Appl. 2021 Oct;129:112372.

39. Xie H, Ruan S, Zhao M, Long J, Ma X, Guo J, et al. Preparation and characterization of 3D hydroxyapatite/collagen scaffolds and its application in bone regeneration with bone morphogenetic protein-2. RSC Adv. 2023 Jul;13(33):23010–20.

40. Li J, Wang M, Qiao Y, Tian Y, Liu J, Qin S, et al. Extraction and characterization of type I collagen from skin of tilapia (Oreochromis niloticus) and its potential application in biomedical scaffold material for tissue engineering. Process Biochem. 2018;74:156–63.

41. Guan Y, He J, Chen J, Li Y, Zhang X, Zheng Y, et al. Valorization of Fish Processing By-Products: Microstructural, Rheological, Functional, and Properties of Silver Carp Skin Type I Collagen. Foods. 2022;11(19).

42. Zhang Q, Lu H, Kawazoe N, Chen G. Pore size effect of collagen scaffolds on cartilage regeneration. Acta Biomater. 2014 May;10(5):2005–13.

43. Ahmadian M, Khoshfetrat AB, Khatami N, Morshedloo F, Rahbarghazi R, Hassani A, et al. Influence of gelatin and collagen incorporation on peroxidase-mediated injectable pectin-based hydrogel and bioactivity of fibroblasts. J Biomater Appl. 2021 Jul;36(1):179–90.

44. Abdulghani S, Mitchell GR. Biomaterials for In Situ Tissue Regeneration: A Review. Biomolecules. 2019 Nov;9(11).

45. Kim H, Kumbar SG, Nukavarapu SP. Biomaterial-directed cell behavior for tissue engineering. Curr Opin Biomed Eng. 2021 Mar;17.

46. Oslan SNH, Li CX, Shapawi R, Mokhtar RAM, Noordin WNM, Huda N. Extraction and Characterization of Bioactive Fish By-Product Collagen as Promising for Potential Wound Healing Agent in Pharmaceutical Applications: Current Trend and Future Perspective. Int J food Sci. 2022;2022:9437878.

47. Chen J, Li L, Yi R, Xu N, Gao R, Hong B. Extraction and characterization of acid-soluble collagen from scales and skin of tilapia (Oreochromis niloticus). Lwt. 2016;66:453–9.

48. Veeruraj A, Arumugam M, Ajithkumar T, Balasubramanian T. Isolation and characterization of drug delivering potential of type-I collagen from eel fish Evenchelys macrura. J Mater Sci Mater Med. 2012;23(7):1729–38.

49. Iglesias-Mejuto A, García-González CA. 3D-printed alginate-hydroxyapatite aerogel scaffolds for bone tissue engineering. Mater Sci Eng C. 2021;131(July).

50. Pati F, Datta P, Adhikari B, Dhara S, Ghosh K, Das Mohapatra PK. Collagen scaffolds derived from fresh water fish origin and their biocompatibility.

J Biomed Mater Res A. 2012 Apr;100(4):1068–79.

51. Han J, Zhou Z, Yin R, Yang D, Nie J. Alginate-chitosan/hydroxyapatite polyelectrolyte complex porous scaffolds: Preparation and characterization. Int J Biol Macromol. 2010;46(2):199–205.

52. Slimane E Ben, Sadok S. Collagen from cartilaginous fish by-products for a potential application in bioactive film composite. Mar Drugs. 2018;16(6).

53. Ali AF, Alrowaili ZA, El-Giar EM, Ahmed MM, El-Kady AM. Novel green synthesis of hydroxyapatite uniform nanorods via microwave-hydrothermal route using licorice root extract as template. Ceram Int. 2021;47(3):3928–37.

54. Zhao Y, Chen H, Ran K, Zhang Y, Pan H, Shangguan J, et al. Porous hydroxyapatite scaffold orchestrated with bioactive coatings for rapid bone repair. Biomater Adv. 2023;144(October 2022):213202.

55. Li S, Li G, Lian X, Hu J, Li M, Wang B, et al. Integrated porous polyetheretherketone/hydroxyapatite scaffolds: design, manufacturing and performance evaluation. Compos Part A Appl Sci Manuf. 2023;173:107656.

56. Afzali M, Boateng JS. Composite Fish Collagen-Hyaluronate Based Lyophilized Scaffolds Modified with Sodium Alginate for Potential Treatment of Chronic Wounds. Polymers (Basel). 2022 Apr;14(8).

57. Oryan A, Baghaban Eslaminejad M, Kamali A, Hosseini S, Sayahpour FA, Baharvand H. Synergistic effect of strontium, bioactive glass and nano-hydroxyapatite promotes bone regeneration of critical-sized radial bone defects. J Biomed Mater Res B Appl Biomater. 2019 Jan;107(1):50–64.

58. Lim HK, Byun SH, Woo JM, Kim SM, Lee SM, Kim BJ, et al. Biocompatibility and Biocorrosion of Hydroxyapatite-Coated Magnesium Plate: Animal Experiment. Mater (Basel, Switzerland). 2017 Sep;10(10).

59. Qi X, Ye J, Wang Y. Improved injectability and in vitro degradation of a calcium phosphate cement containing poly(lactide-co-glycolide) microspheres. Acta Biomater. 2008 Nov;4(6):1837–45.

60. Ruhé PQ, Hedberg EL, Padron NT, Spauwen PHM, Jansen JA, Mikos AG. Biocompatibility and degradation of poly(DL-lactic-co-glycolic acid)/calcium phosphate cement composites. J Biomed Mater Res A. 2005 Sep;74(4):533–44.

61. Van de Watering FCJ, van den Beucken JJJP, Walboomers XF, Jansen JA. Calcium phosphate/poly(D,L-lactic-co-glycolic acid) composite bone substitute materials: evaluation of temporal degradation and bone ingrowth in a rat critical-sized cranial defect. Clin Oral Implants Res. 2012 Feb;23(2):151–9.

62. Parisi JR, Fernandes KR, Avanzi IR, Dorileo BP, Santana AF, Andrade AL, et al. Incorporation of Collagen from Marine Sponges (Spongin) into Hydroxyapatite Samples: Characterization and In Vitro Biological Evaluation. Mar Biotechnol. 2019 Feb 15;21(1):30–7.

63. Lu HH, Tang A, Oh SC, Spalazzi JP, Dionisio K. Compositional effects on the formation of a calcium phosphate layer and the response of osteoblast-like cells on polymer-bioactive glass composites. Biomaterials. 2005 Nov;26(32):6323–34.

64. Välimäki VV, Yrjans JJ, Vuorio EI, Aro HT. Molecular biological evaluation of bioactive glass microspheres and adjunct bone morphogenetic protein 2 gene transfer in the enhancement of new bone formation. Tissue Eng. 2005;11(3–4):387–94.

65. Magri AMP, Fernandes KR, Ueno FR, Kido HW, da Silva AC, Braga FJC, et al. Osteoconductive properties of two different bioactive glass forms (powder and fiber) combined with collagen. Appl Surf Sci. 2017 Nov 30;423:557–65.

66. Eshkol-Yogev I, Tobias T, Keren A, Gilhar A, Gilboa E, Furer A, et al. Dual composite bioadhesives for wound closure applications: An in vitro and in vivo study. Polym Adv Technol. 2022 Nov;33(11):3862–77.

67. Scarano A, Lorusso F, Staiti G, Sinjari B, Tampieri A, Mortellaro C. Sinus Augmentation with Biomimetic Nanostructured Matrix: Tomographic, Radiological, Histological and Histomorphometrical Results after 6 Months in Humans. Front Physiol. 2017;8:565.

68. Ramírez-Rodríguez GB, Delgado-López JM, Iafisco M, Montesi M, Sandri M, Sprio S, et al. Biomimetic mineralization of recombinant collagen type I derived protein to obtain hybrid matrices for bone regeneration. J Struct Biol. 2016 Nov;196(2):138–46.

69. Kwak HB. Aging, exercise, and extracellular matrix in the heart. J Exerc Rehabil. 2013;9(3):338–47.

70. Furtado M, Chen L, Chen Z, Chen A, Cui W. Development of fish collagen in tissue regeneration and drug delivery. Eng Regen.

2022;3(3):217–31.

71. Rajabimashhadi Z, Gallo N, Salvatore L, Lionetto F. Collagen Derived from Fish Industry Waste: Progresses and Challenges. Polymers (Basel). 2023 Jan;15(3).

72. Veiga A, Castro F, Rocha F, Oliveira AL. An update on hydroxyapatite/collagen composites: What is there left to say about these bioinspired materials? J Biomed Mater Res Part B Appl Biomater. 2022 May 1;110(5):1192–205.

73. Habibovic P, Sees TM, van den Doel MA, van Blitterswijk CA, de Groot K. Osteoinduction by biomaterials--physicochemical and structural influences. J Biomed Mater Res A. 2006 Jun;77(4):747–62.

74. Laurenti KC, Haach LC de A, Santos Jr. AR dos, Rollo JMD de A, Reiff RB de M, Gaspar AMM, et al. Cartilage reconstruction using self-anchoring implant with functional gradient. Vol. 17, Materials Research. scielo ; 2014.

75. Lu HH, El-Amin SF, Scott KD, Laurencin CT. Three-dimensional, bioactive, biodegradable, polymer-bioactive glass composite scaffolds with improved mechanical properties support collagen synthesis and mineralization of human osteoblast-like cells in vitro. J Biomed Mater Res A. 2003 Mar;64(3):465–74.